Superresolution vibrational imaging by simultaneous detection of Raman and hyper-Raman scattering

Korenobu Matsuzaki,[1] Rintaro Shimada,[1] and Hiro-o Hamaguchi[1,2,*]

[1]*Department of Chemistry, School of Science, The University of Tokyo, 7-3-1 Hongo, Bunkyo-ku, Tokyo 113-0033, Japan*

[2]*Institute of Molecular Science and Department of Applied Chemistry, National Chiao Tung University, 1001 Ta Hsueh Road, Hsinchu 300, Taiwan*

**Corresponding author: hhama@chem.s.u-tokyo.ac.jp*

Received March 31, 2011; revised June 4, 2011; accepted June 6, 2011; posted June 7, 2011 (Doc. ID 145139); published July 1, 2011

We have developed a superresolution vibrational imaging method by simultaneous detection of Raman and hyper-Raman scattering. Raman and hyper-Raman images obtained with the same laser spot carry independent information on the sample spatial distribution, owing to different signal dependence (linear in Raman and quadratic in hyper-Raman) on the incident light intensity. This information can be quantitatively analyzed to recover the incident light intensity distribution at the focal plane. A superresolution vibrational image is then derived by the constrained deconvolution of the images by the obtained incident light intensity distribution. This method has been applied to a TiO_2 nanostructure and the obtained superresolution image was compared with a scanning electron microscopy image. The spatial resolution achieved by the present method is evaluated to be 160 nm, which is more than twice better than the diffraction limited resolution.

OCIS codes: 100.1830, 100.6640, 180.5655, 300.6330.

Spatial resolution beyond the diffraction limit (superresolution) has always been a challenge in microscopy and microspectroscopy. Superresolution enables us to study the fine structures that are not accessible by conventional microscopy. In the past decade, superresolution techniques such as stimulated-emission-depletion microscopy [1,2], stochastic optical reconstruction microscopy (STORM) [3], and deconvolution microscopy [4] have been developed based on fluorescence microscopy. There has also been an attempt to achieve superresolution in Raman microscopy [5]. In this Letter, we report on a novel superresolution technique based on Raman and hyper-Raman microspectroscopy. It can provide us with a superresolution image by a single measurement in which Raman and hyper-Raman images are acquired simultaneously. Separate measurements of the standard samples, such as polystyrene beads [5], are not required.

Raman microspectroscopy is the combination of microscopy with Raman spectroscopy. It enables us to study the chemical composition and its distribution in a sample under a microscope, on the basis of vibrational spectroscopy. The spatial resolution of Raman microspectroscopy is diffraction limited; when the excitation wavelength is 755 nm and the NA of the objective lens is 1.30, as in the case of the current study, the diffraction limited spatial resolution is $0.61\lambda/\mathrm{NA} = 350\,\mathrm{nm}$ [6]. Hyper-Raman microspectroscopy [7], on the other hand, is the combination of microscopy with hyper-Raman spectroscopy [8]. Hyper-Raman spectroscopy is a two-photon excited analog of Raman spectroscopy that detects a new radiation generated near the second harmonic of the incident laser light. Since hyper-Raman scattering is a two-photon excited process, its intensity scales quadratically to the incident light intensity. Owing to this nonlinearity, hyper-Raman microspectroscopy achieves spatial resolution superior to Raman microspectroscopy by a factor of $\sqrt{2}$ [9]. Nonetheless, it cannot be made significantly better than the diffraction limit.

We here show that the diffraction limit can be overcome by combining Raman microspectroscopy with hyper-Raman microspectroscopy. Since Raman and hyper-Raman scattering intensities have different dependence on the incident light intensity, resulting Raman and hyper-Raman images show different extent of "blur". Through the combined analysis of these two differently blurred images, we can determine the incident light intensity and the true distribution of sample molecules. That is to say, we can achieve superresolution by quantitatively comparing Raman and hyper-Raman images. This is the principle of the present method.

Raman and hyper-Raman images obtained by raster scanning can be expressed in the incoherence limit [10] as

$$R = \chi * I, \qquad H = \chi * I^2, \tag{1}$$

where $R(x,y)$ and $H(x,y)$ are Raman and hyper-Raman images, respectively, $\chi(x,y)$ and $I(x,y)$ are the sample distribution and the incident light intensity on the focal plane, respectively, and asterisks $(*)$ denote two-dimensional convolution. Coordinates (x,y) have been omitted from the equations for simplicity. In the second equation, $I^2(x,y)$ is used instead of $I(x,y)$ because hyper-Raman scattering intensity is proportional to the square of the incident light intensity. Our goal is to determine $\chi(x,y)$ as accurately as possible. In this formulation, we took only the two-dimensional structure of the sample into account. This simplification is valid if the sample is thinner than the focal depth of the objective lens, as in the case of the current experiment.

First, we determine the incident light intensity $I(x,y)$ by eliminating $\chi(x,y)$ from Eqs. (1). This can be done by convolving $I^2(x,y)$ to the first equation and $I(x,y)$ to the second equation:

$$R * I^2 = H * I = \chi * I * I^2. \tag{2}$$

In principle, $I(x,y)$ can be obtained by solving this equation. However, this equation is ill-posed and cannot

be solved as it is. If we try to do so, the solution will be contaminated by artifacts arising from the noise present in $R(x,y)$ and $H(x,y)$, and the solution will eventually converge to $I(x,y)=0$. In order to avoid this, we introduce Tikhonov regularization [11]; we obtain $I(x,y)$ by solving the following least squares problem:

$$\varepsilon = |R * I^2 - H * I|^2 + \gamma |I - I_0|^2. \tag{3}$$

Here, γ is the regularization parameter, which is determined by the L-curve method [12], and $I_0(x,y)$ is an approximated solution to Eq. (2) obtained under the assumption that $I(x,y)$ can be expressed by a Gaussian function. A Gaussian function was chosen because Eq. (2) readily yields an analytical solution if $I(x,y)$ is a Gaussian. By solving the least squares problem under the nonnegative constraint ($I(x,y) \geq 0$) using the gradient projection method [13], $I(x,y)$ can be obtained.

Next, we determine the sample distribution $\chi(x,y)$ by the deconvolution of $R(x,y)$ and $H(x,y)$. Theoretically, it is sufficient to use only one of the equations in Eqs. (1) to obtain $\chi(x,y)$. However, we found that, by using both of the equations simultaneously for deconvolution, better spatial resolution can be achieved because the noise present in $R(x,y)$ and $H(x,y)$ can be efficiently suppressed. This simultaneous deconvolution can be implemented by the following least squares problem:

$$\varepsilon = |R - \chi * I|^2 + |H - \chi * I^2|^2 + \gamma |\chi|^2. \tag{4}$$

Here, first two terms are for the deconvolution of $R(x,y)$ and $H(x,y)$, and the last term is for Tikhonov regularization. As in Eq. (3), γ is the regularization parameter and is determined by the L-curve method [12]. Furthermore, nonnegative constraint ($\chi(x,y) \geq 0$) is imposed on $\chi(x,y)$. Solving this least squares problem by the gradient projection method [13], sample distribution $\chi(x,y)$ can be determined, with spatial resolution beyond the diffraction limit.

In order to use the procedure given above, Raman and hyper-Raman images must be obtained simultaneously using the common $I(x,y)$. This was done by a laboratory-made simultaneous Raman and hyper-Raman microspectroscopic imaging system (Fig. 1). The excitation light source is a picosecond mode-locked Ti:sapphire oscillator (755 nm, 3 ps, 82 MHz) pumped by a cw 532 nm Nd:YVO_4 laser. Average power at the sample position is adjusted to 20 mW by a variable neutral density filter. The excitation light is introduced into an inverted microscope, and is focused onto the sample by an objective lens (40×, NA 1.30). Raman and hyper-Raman scattering generated at the focal position is collected by the same objective lens in the backscattering configuration. Raman scattering is separated from the excitation light by a laser line filter and two edge filters, introduced into a polychromator via optical fiber, dispersed in the polychromator, and detected by a CCD camera. Hyper-Raman scattering is separated from the incident light by a dichroic mirror and a color glass filter, dispersed in a polychromator, and detected by a CCD camera. The sample stage is equipped with a piezo stage, and the sample can be raster scanned to give Raman and hyper-Raman images simultaneously. Laser output and the intensity of the second harmonic generated by a beta-barium borate crystal are monitored inside the autocorrelator in Fig. 1 throughout the imaging experiment, in order to make corrections to the intensities of Raman and hyper-Raman scattering, respectively. This allows us to eliminate the effect of laser intensity and pulse duration fluctuation.

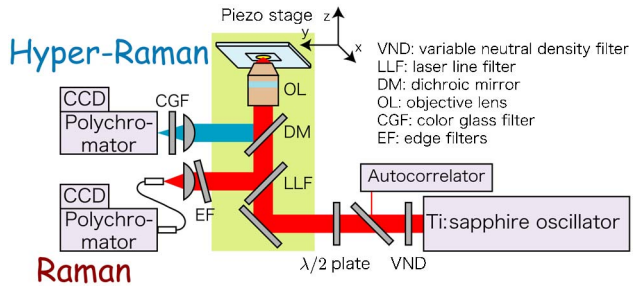

Fig. 1. (Color online) Simultaneous Raman and hyper-Raman microspectroscopic imaging system.

The sample used in the present study was a TiO_2 nanostructure prepared by etching a TiO_2 (anatase) thin film on a glass plate by photolithography. Its thickness was 170 nm. The film showed an isotropic polarized microscope image in crossed-Nichol configuration, indicating that it comprises randomly oriented nanocrystals. Raster scan imaging was done within the area of 4 μm × 4 μm by 70 nm pitch point-by-point measurements (57 points × 57 points). Exposure time was 3 s for each sample point, and the total acquisition time for Raman and hyper-Raman images was 3 h.

Figure 2 shows Raman and hyper-Raman spectra of anatase-type TiO_2. All of the observed bands are assigned to the lattice vibrations of anatase-type TiO_2 [14,15]. By using the Raman band at 144 cm^{-1} and the broad hyper-Raman band centered at 850 cm^{-1}, Raman and hyper-Raman images were obtained as in Figs. 3(a) and 3(b). The direction of the y axis was chosen so that it coincides with the polarization direction of the incident light electric field. Through the procedure described above, the incident light intensity distribution was first determined [Fig. 3(c)], followed by the superresolution image [Fig. 3(d)]. From the comparison with the observed Raman and hyper-Raman images, we can easily see the improvement of the spatial resolution in Fig. 3(d). Figure 3(e) shows the scanning electron microscopy (SEM) image of the sample.

To evaluate the improvement of spatial resolution quantitatively, intensity cross sections along the dotted

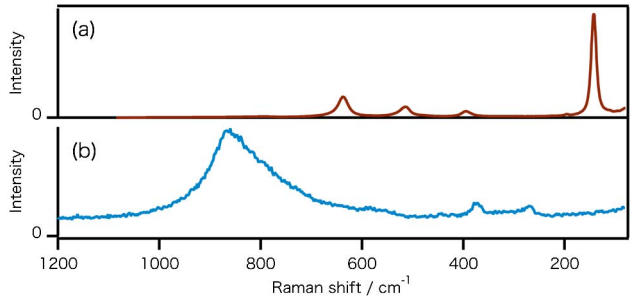

Fig. 2. (Color online) (a) Raman and (b) hyper-Raman spectra of anatase-type TiO_2.

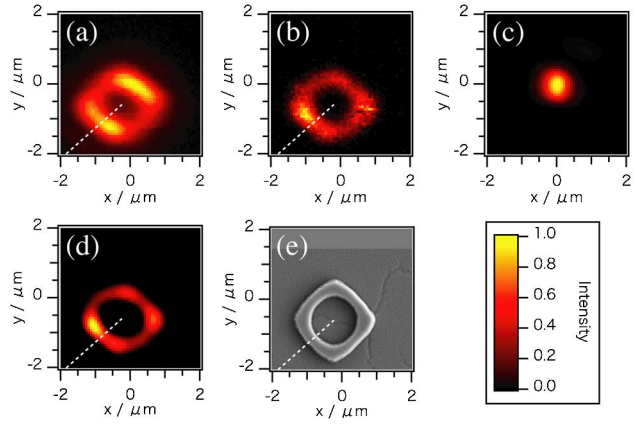

Fig. 3. (Color online) (a) Raman and (b) hyper-Raman images of the TiO_2 standard sample, (c) incident light intensity distribution, (d) superresolution, and (e) SEM images of the TiO_2 standard sample.

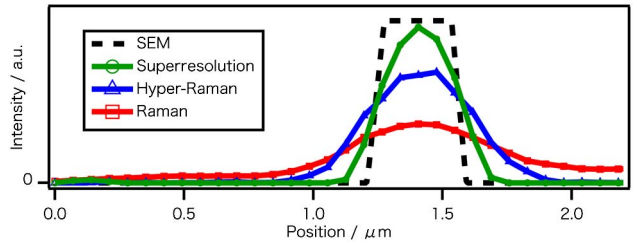

Fig. 4. (Color online) Intensity cross sections of Raman, hyper-Raman, superresolution, and SEM images along the dotted lines in Fig. 3.

lines indicated in Figs. 3(a), 3(b), 3(d), and 3(e) are examined (Fig. 4). Assuming that the SEM image shows the true shape of the sample and the degradation of the spatial resolution can be expressed by a Gaussian function, each of the cross sections in Fig. 4 are fitted by the convolution of a Gaussian and the SEM cross section, and the spatial resolution is obtained as the FWHM of the Gaussian. The spatial resolution determined in this manner was 620 nm for the Raman image, 390 nm for the hyper-Raman image, and 160 nm for the superresolution image. As is stated above, the diffraction limited spatial resolution of the current system is 350 nm, and we have succeeded in achieving a spatial resolution more than twice better than the diffraction limited resolution.

Although we were able to achieve superresolution, we failed to reproduce the uniformity of the sample thickness, as can be seen in the SEM image [Fig. 3(e)]. This failure probably comes from the fact that we have naively assumed in Eqs. (1) that Raman and hyper-Raman scattering intensity is always proportional to the quantity of the sample, which is not true when, for example, the crystal axis is not in the same direction everywhere inside the sample. From the viewpoint of examining sample morphology, this fact limits the present method but it contains extra information, for example, on crystal orientation that SEM can never provide. Thus, the current method is complementary with SEM and other scanning microscopy methods.

In conclusion, we have developed a superresolution vibrational imaging method based on simultaneous detection of Raman and hyper-Raman scattering. This is a unique superresolution technique that provides us with both detailed molecular information characteristic of vibrational spectroscopy and sub-diffraction-limited spatial resolution of 160 nm at the same time, through *in situ* and noninvasive measurement without any pretreatments. This method will open up new possibilities for studying detailed molecular properties of microstructures that have not, so far, been accessible by existing fluorescence superresolution techniques.

The authors acknowledge Prof. Tetsuya Hasegawa and Prof. Yasuo Wada for their help in sample preparation. Part of this study was conducted with support from the Toyo University Nanotechnology Network, which is part of the Nanotechnology Network Japan by the Ministry of Education, Culture, Sports, Science and Technology.

References

1. S. W. Hell and J. Wichmann, Opt. Lett. **19**, 780 (1994).
2. T. A. Klar and S. W. Hell, Opt. Lett. **24**, 954 (1999).
3. M. J. Rust, M. Bates, and X. Zhuang, Nat. Meth. **3**, 793 (2006).
4. J. G. McNally, T. Karpova, J. Cooper, and J. A. Conchello, Methods **19**, 373 (1999).
5. J. Ling, S. D. Weitman, M. A. Miller, R. V. Moore, and A. C. Bovik, Appl. Opt. **41**, 6006 (2002).
6. E. Hecht, *Optics*, 4th ed. (Addison-Wesley, 2002), p. 472.
7. R. Shimada, H. Kano, and H. Hamaguchi, Opt. Lett. **31**, 320 (2006).
8. R. W. Terhune, P. D. Maker, and C. M. Savage, Phys. Rev. Lett. **14**, 681 (1965).
9. J. Squier and M. Muller, Rev. Sci. Instrum. **72**, 2855 (2001).
10. T. Wilson and C. Sheppard, *Theory and Practice of Scanning Optical Microscopy* (Academic, 1984), p. 39.
11. B. Hofmann and L. v. Wolfersdorf, Numer. Funct. Anal. Optim. **27**, 357 (2006).
12. P. C. Hansen and D. P. O'Leary, SIAM J. Sci. Comput. **14**, 1487 (1993).
13. O. Nakamura, S. Kawata, and S. Minami, J. Opt. Soc. Am. A **5**, 554 (1988).
14. T. Ohsaka, F. Izumi, and Y. Fujiki, J. Raman Spectrosc. **7**, 321 (1978).
15. R. J. Gonzalez, R. Zallen, and H. Berger, Phys. Rev. B **55**, 7014 (1997).